is formed at the center of the twin. The dislocations enter this region with small velocities. As is known,[1] the intensity of the annihilation emission is proportional to the velocity of the approaching dislocations. This can explain the absence of contraction of the twin in the initial states. As the twin contracts, d decreases. At $d \sim r_a$ (r_a is the annihilation radius), the dislocations begin to enter into the reaction with high velocity, which leads to the appearance of intense sound emission. Using the experimental data and the results of Ref. 5, we can obtain an estimate of the annihilation radius:

$$r_a \sim (MA/\mu) L_u^{1/2}, \quad (2)$$

where M is the phenomenological parameter of the theory of Ref. 6 and characterizes the surface tension, A is a dimensionless constant, μ is the shear modulus, L_u is the half-length of the twin, corresponding to the appearance of sound emission [$M \sim 1$ kg/cm$^{3/2}$ (Ref. 6), $A \sim 10^{-1}$ (Ref. 5), $\mu \sim 10^5$ kg/cm^2]. Taking it into account that, according to the experimental data, the sound emission begins at $L_u \sim 10^{-1}$ cm, we obtain the results that the annihilation radius of twinning dislocations can be estimated at $r_a \sim 10^{-7}$ cm. This result agrees with the data of the mathematical model.[4] It should be noted, of course, that this is a lower-bound estimate.

In conclusion, we take this opportunity to express our deep gratitude to R. I. Garber for discussion of the results, and also V. D. Natsik for useful discussions.

[1)]The direction of arrival of the sound wave is kept fixed at such a placement of the pickup relative to the emission source.

[1]V. D. Natsik and K. A. Chishko, Fiz. Tverd. Tela (Leningrad) **14**, 3126 (1972) [Sov. Phys. Solid State **14**, 2678 (1973)].
[2]V. S. Boĭko, R. I. Garber, V. F. Kivshik, and L. F. Krivenko, Zh. Eksp. Teor. Fiz. **71**, 708 (1976) [Sov. Phys. JETP **44**, 372 (1976)].
[3]V. S. Boĭko, R. I. Garber, and L. F. Krivenko, Fiz. Tverd. Tela (Leningrad) **16**, 1233 (1974) [Sov. Phys. Solid State **16**, 798 (1975)].
[4]V. S. Boĭko, in sbornik (collection) Defekty v metallkh i ikh modelirovanie na ÉVM (Defects in metals and their modeling on a computer) Yu. A. Osip'yan, ed., Nauka, 1980, Ch. 8.
[5]V. S. Boĭko and A. A. Slutskin, J. Phys. Chem. Sol. **38**, 1221 (1977).
[6]A. M. Kosevich and V. S. Boĭko, Usp. Fiz. Nauk **104**, 201 (1974) [Sov. Phys. Uspekhi **14**, 286 (1971)].

Translated by R. T. Beyer

Diffraction focusing by a bent perfect crystal

O. I. Sumbaev and E. G. Lapin

Leningrad Institute of Nuclear Physics, USSR Academy of Sciences
(Submitted 8 August 1979)
Zh. Eksp. Teor. Fiz. **78**, 803–812 (February 1980)

The diffraction focusing effect described by Afanas'ev and Kon [Sov. Phys. Solid State **19**, 1035 (1977)] for an undeformed perfect crystal is considered for the more general case of an elastically bent ideal crystal with reflecting planes that are bent as a result of the anisotropy [O. I. Sumbaev, Crystal-diffraction gamma spectrometry, Atomizdat (1963); Sov. Phys. JETP **27**, 724 (1968)] within the framework of the Kato eikonal dynamic theory [J. Phys. Soc. Jpn., **19**, 1971 (1964)]. An experiment performed in the geometry of a two-crystal x-ray spectrometer has confirmed the presence of substantial dynamic effects, and yielded quantitative agreement with calculation. By way of applications, the following are calculated: a Cauchois focusing diffraction spectrometer; "point-into-point" focusing of the type considered by Petrashen' and Chukhovskii [Preprint, Crystallography Institute, USSR Academy of Sciences, 1975; JETP Lett. **23**, 347 (1976)], and "point-into-parallel beam" focusing.

PACS numbers: 78.70.Ck, 61.10.Dp

INTRODUCTION

Authier *et al.*[1] and Ibdenbom and co-authors described the effect of focusing of diffracted x-ray (or neutron) radiation inside a perfect flat crystal. Petrashen' and Chukhovskii[3] described an analogous effect in an elastically bent crystal. Recently Afanas'ev and Kon[4] considered theoretically, and others soon observed experimentally,[5,6] the effect of focusing of x radiation diffracted by a flat perfect crystal at a distance of several meters behind the crystal. After studying Refs. 4–6, we noted that the described effect can be easily generalized to include the case of an elastically deformed perfect crystal, including one with bent reflecting surfaces, within the framework of the Kato eikonal theory.[7]

1. DERIVATION OF FUNDAMENTAL RELATIONS

We consider (Fig. 1) diffraction, by a crystal, of radiation emitted by a point source S located near the crystal surface. We shall consider the symmetrical case of Laue diffraction, when the diffracting planes in question coincide with the normal cross sections of the initial (prior to the elastic bending) plane-parallel single-crystal plate. If the crystal is elastically bent into a cylindrical surface of radius ρ, the reflecting planes also are bent, generally speaking, into cylinders (parabolas) of radius ρ' given by (see, e.g., Refs. 8 and 9)

$$\rho' = \frac{1}{2k}, \quad k \approx \frac{1}{2\rho} \frac{a_{34} - a_{45}a_{35}/a_{55}}{a_{33} - a_{35}^2/a_{55}}. \quad (1)$$

 0038-5646/80/020403-06$02.40

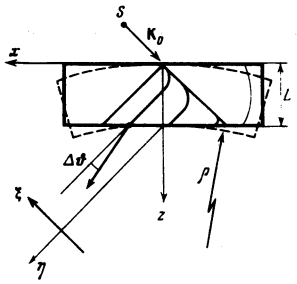

FIG. 1. Diffraction of X radiation emitted by point source S located near the entrance face of a single-crystal plate of thickness L, bent into a cylinder of radius ρ and thickness L and having reflecting planes that coincide prior to the bending with the normal cross sections.

Here a_{ij} are the components of the elastic tensor of the crystal.

The symmetrical case seems theoretically most attractive to us, and furthermore it is most frequently encountered in the practice of focusing diffraction spectrometers. It is easy to show that the problem reduces to the solution considered by Kato, with the constant "force" now defined by the relation

$$f=\frac{2\pi}{d}\frac{k}{\operatorname{tg}\vartheta} \tag{2}$$

(here ϑ is the Bragg angle and d is the interplanar distance between the employed system of reflecting planes). It remains for us only to continue the rays described by Kato inside the crystal beyond the exit face of the crystal. In this case we shall deal from the very outset intensities rather than amplitudes, to avoid interference effects. The latter greatly complicate the formulas, but at the parameters encountered in practice they are usually, in final analysis, "integrated out" by the finite width of the sources and detectors.[1)]

To find the trajectory of the ray emerging from the crystal through a point on the lower face with coordinates $z=L, x$ it is necessary only to determine the angle $\Delta\vartheta$ of its deviation from the exact Bragg direction, which in our figure is the η axis. This can be easily done by taking into account the boundary conditions on the exit face, i.e., by starting from the usual condition of conservation of the tangential component of the wave vectors (Fig. 2). A simple geometrical procedure connects the angle $\Delta\vartheta_a$ of the deflection of a certain diffracted ray K, propagating behind the crystal, with the angle of inclination φ of the corresponding Kato trajectory at the exit face inside the crystal:

$$\operatorname{tg}\varphi=\pm\frac{K\sin^2\vartheta\Delta\vartheta_a}{\cos\vartheta[D^2/4+(\Delta\vartheta_a K\sin\vartheta)^2]^{1/2}}. \tag{3}$$

Here D is the diameter of the dispersion α and β hyperbolas. Solving (3) with respect to $\Delta\vartheta_a$, taking into account the Bragg condition $K=\pi/d\sin\vartheta$ and the relation $D=2m_0\operatorname{tg}\vartheta$, introducing the Kato dimensionless parameters X and Z by means of the relation (see Ref. 7, 36a)

$$\operatorname{tg}\varphi/\operatorname{tg}\vartheta=(Z+Z_0)/(X+X_0)$$

and eliminating X_0 and Z_0 by means of the relations (see Ref. 7, 32 and 33)

$$(X+X_0)^2-(Z+Z_0)^2\neq 1,\quad X_0^2-Z_0^2=1,$$

we obtain[2)]

$$\frac{\Delta\vartheta_a}{kL}=\pm\frac{X}{Z}\frac{\tau}{\sigma}. \tag{3'}$$

Here

$$X=\left(\frac{f}{m_0}\right)\frac{x}{\operatorname{tg}\vartheta},\quad Z=\left(\frac{f}{m_0}\right)L,\quad \sigma=\frac{1}{2}(Z^2-X^2),$$
$$\tau=\frac{1}{2}[(Z^2-X^2+4)(Z^2-X^2)]^{1/2},$$

k and f are specified by relations (1) and (2) above,

$$m_0=2r_e d(F_g F_{\bar g})^{1/2}V^{-1}\cos\pi^*$$

is the effective Kato "mass" (see Ref. 7, 2b), r_e is the classical radius of the electron, d and F_g are the interplanar distance and the structure factor of the employed system of planes, V is the volume of the unit cell of the crystal, and $\cos\pi^*$ is a polarization parameter equal to unity or to $\cos 2\vartheta$ for σ and π polarization, respectively.

In addition to this diffractive deflection, there exists also a trivial effect due to the rotation of the rays simply on account of the bending of the outer face of the crystal (see Fig. 1, dashed):

$$\Delta\vartheta_\rho=\pm\frac{x}{\rho}=\pm\frac{LX}{Z}\frac{\operatorname{tg}\vartheta}{\rho}.$$

Thus, the total deflection of the beam diffracted by the cylindrically bent crystal of radius ρ and with the normal reflecting planes bent on account of anisotropy with a bending coefficient k, is given by the relation

$$\Delta\vartheta_\Sigma=\frac{LX}{Z}\left((\pm)\frac{\operatorname{tg}\vartheta}{\rho}\pm k\frac{\tau}{\sigma}\right). \tag{4}$$

The plus and minus signs in front of the first term indicate the direction of the bending of the crystal (the minus sign corresponds to the situation of Fig. 1, when the concave side of the crystal faces the detector), while the signs + and − in front of the second term pertain to the α or β branches [see Fig. 2 and relation (3)].

It is now easy to find the coordinate ξ of the point where the ray x, L (or X, Z in the Kato dimensionless coordinates), intersects a screen perpendicular to the η axis and located at a distance η away from the crystal:

$$\xi(X,\eta)=\frac{LX}{Z}\left(\sin\vartheta-\frac{\eta}{\rho}\operatorname{tg}\vartheta\mp k\eta\frac{\tau}{\sigma}\right). \tag{5}$$

The intensity of the diffracted ray is given by Kato by relation 44b.[7] We reduce it to a form more convenient

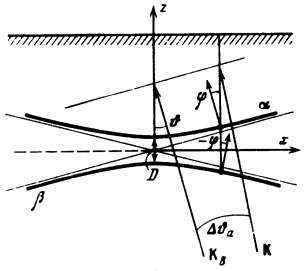

FIG. 2. Illustrating the derivation of the connection between the deviation $\Delta\vartheta_a$ of the diffracted beam K emerging from the crystal from the Bragg direction, on the one hand, and the propagation direction φ of the Kato ray at the exit face inside the crystal, which coincides with the normal to the dispersion α and β hyperbolas, on the other.

for our purposes, by changing from $dI/d\xi$ (at $z=L$), which was used in Kato's formula, to dI/dX, and by introducing directly the total activity (the number of photons emitted per unit time in an angle 4π) of the source N:

$$\frac{dI}{dX}=\frac{N}{4\pi}\exp\left\{-\frac{\mu L}{\cos\vartheta}\right\}e^{2iS}\Delta\varphi_v\Delta\vartheta_B\frac{1+\sigma\pm|\tau|}{8|\tau|}, \tag{6}$$

where μ is the linear coefficient of absorption of the radiation by the crystal

$$2S=\pm P\,\mathrm{arc\,sh}\left(\frac{\sigma}{2}\right)^{1/2},\quad P=\frac{2\cos\pi^*}{\cos\vartheta}\frac{\mu\varepsilon L}{Z},$$

ε is the ratio of the imaginary structure factors at the Bragg angle and in the forward direction, $\Delta\varphi_v$ is the angle in the vertical plane at which the detector is seen from the source, and $\Delta\vartheta_B$ is the standard Bragg diffraction width for an ideal flat crystal.

In relation (6), $(N/4\pi)\Delta\varphi_B\Delta\vartheta_B$ obviously determines the number of quanta per second traveling within the confines of the vertical $\Delta\varphi_v$ in the standard $\Delta\vartheta_B$ horizontal apertures, while the exponential factors take into account the normal and anomalous absorption (the plus sign in the expression for $2S$ corresponds to the α branch). Finally, the right-hand fraction takes into account the singularities of the diffraction on the bent crystal (the plus sign corresponds here to the so called essential Kato mode, and the minus sign to the inessential one[3)]).

We write down also an expression for the derivatives of $\Delta\vartheta_D$ and ξ with respect to X:

$$\frac{d\Delta\vartheta_x}{dX}=(\pm)\frac{L}{Z}\frac{\mathrm{tg}\,\vartheta}{\rho}\pm\frac{L}{Z}k\frac{\sigma^2+Z^2}{\sigma\tau}, \tag{7}$$

$$\frac{d\xi}{dX}=\frac{L}{Z}\left(\sin\vartheta-\eta\frac{\mathrm{tg}\,\vartheta}{\rho}\mp k\eta\frac{\tau^2+X^2}{\sigma\tau}\right). \tag{8}$$

Equations (4)–(8) obviously make it easy to calculate the distributions that are of importance for the experiments. Thus, by specifying a sequence of values of X in the region $|X|<Z$ we obtain, for example, ξ and

$$\frac{dI}{d\xi}\equiv\frac{dI}{dX}\Big/\frac{d\xi}{dX},$$

i.e., the shape of the line $dI/d\xi=f_1(\xi)$ on an arbitrarily remote screen, or $\Delta\vartheta_D$ and

$$\frac{dI}{d\Delta\vartheta_x}\equiv\frac{dI}{dX}\Big/\frac{d\Delta\vartheta_x}{dX}$$

i.e., the angular distribution of the intensity in the diffracted beam: $dI/d\Delta\vartheta_D=f_2(\Delta\vartheta_D)$.

2. EXPERIMENTAL CHECK ON THE THEORY

An experiment performed in the geometry of a two-crystal spectrometer usually turns out to provide the most information, and it is precisely this scheme (see Fig. 3) which was chosen for an experimental check of the developed theory.

The crystal C_1 was a plane-parallel plate of natural quartz, 0.16 cm thick, and reflecting planes $01\bar{1}1$ coinciding with the normal cross sections. The plate was cut in such a way that $k=0.88\cdot10^{-4}$ cm^{-1} (see, e.g., Ref. 8). The plate was clamped between cylindrical steel mirrors and bent at a radius of 2 m. The crystal C_2

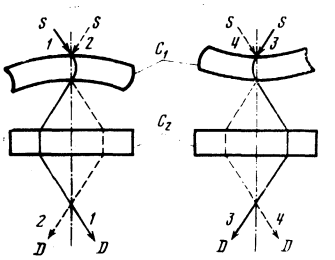

FIG. 3. Arrangement of the crystals $C_{1,2}$, of the source S, and of the detector D in an experimental check on the theory. The investigated variants are numbered 1–4.

was identical with C_1, but remained flat, and the reflection was from the planes $0\bar{1}11$, which had the same d. However since it had approximately half as large a structural factor, it produced a smaller Bragg width ($\Delta\vartheta_B\approx2''$), which determined obviously the angular resolution in our experiment. The radiation source was an x-ray tube with a molybdenum anticathode, and prior collimation ensured reflection of the region of the $K_{\alpha1}$ line of Mo from the crystal C_1. The details of the working spectrum are inessential, since we used a parallel geometry, i.e., without dispersion. The detector was an NaI(Tl) counter with a narrow ($\Delta d\approx4$ mm) receiving slit. Obviously, three positions are possible in the experiment, marked 1–4 in Fig. 3.

The solid lines of Fig. 4 show the results of the calculation by formulas (4), (6), and (7) of the functions $dI/d\Delta\vartheta_D=f(\Delta\vartheta_D)$ for positions 1–4 at the following values of the essential parameters: $Z=4.0$; $P=0.55$; $k=0.88\cdot10^{-4}$ cm^{-1}. The symbols $E(I)\alpha(\beta)$ designate the essential (inessential) Kato modes and the $\alpha(\beta)$ branches. All the pictures are symmetrical about the ordinate axis, and to save space only half of each theoretical curve is shown. All the experimental points are shown, the black ones being those to the left of the ordinate axis.

We point out first of all the rather unexpected variety of shapes and details of the considered picture. When the signs of the first and second terms in relations (4) and (7) are different (this occurs for cases $I\beta1$, $E\beta2$, $E\alpha3$, and $I\alpha4$, then $|\Delta\vartheta_D|$ goes at a certain $X=X_m$ through a maximum, with a value for our parameters $\Delta\vartheta_{Dm}=11.7''$. Obviously $d\Delta\vartheta_D/dX\to0$ and $dI/d\Delta\vartheta_D\equiv(dI/dX)/(d\Delta\vartheta_D/dX)$ diverges (dI/dX has no singularities in the entire region $|X|<Z$; see Ref. 7, Fig. 3). This explains the origin of the characteristic lambda-shaped singularities in Fig. 4. The absolute intensity is determined by the combination of the indices and is obviously maximal for the essential α (i.e., weakly absorbed) mode ($E\alpha3$ in the figure) and minimal for $I\beta1$. The described phenomenon is physically a unique manifestation of diffraction focusing and corresponds to compensation, in a certain region Δx (see Fig. 1) at the bottom of the Bormann delta, of the diffraction increment of the deflection angle, and of the increment due to the bending of the exit face; this cancellation leads to the appearance of two (at $\pm x_m$) almost parallel beams in the directions $\pm\Delta\vartheta_{Dm}$. When the terms in (4) and (7) are of the same sign, as is the case for the remaining four combinations of indices $E\alpha1$, $I\alpha2$, $I\beta3$, and $E\beta4$, the

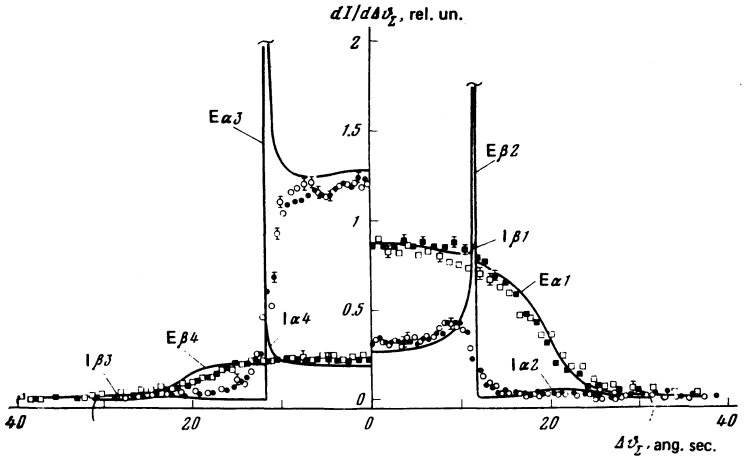

FIG. 4. Comparison of the theoretical (solid lines) and experimental (points) diffraction maxima corresponding to the two-crystal spectrometer of Fig. 3. The markings on the curves (for example, Eα1) designate the essential (E) of inessential (I) Kato modes, the α and β branches, and the variants 1–4 of the arrangement in accordance with Fig. 3.

value of $|\Delta\vartheta_D|$ increases monotonically as $X \to Z$. Broad reflections are produced, and their intensities and shapes are determined by the features of dI/dX (whether the mode is essential or inessential), and also by the sign of the anomalous absorption and its dependence on X (i.e., on $\Delta\vartheta_D$). On the whole, the experimental points fit quite well the theoretical curves. (The experimental intensities are expressed in units of the intensity of the experimental curve 1 at $\Delta_D = 0$, which is made to coincide with the corresponding intensity of the theoretical curve 1.) A quantitative comparison is made in the table for the total width at half height ($\Delta_{1/2}$) and for the relative intensities at zero.[4)]

3. APPLICATIONS TO THE THEORY OF FOCUSING INSTRUMENTS

A. Cauchois spectrometer

Equations (4)–(7) make it easy to formulate an almost sufficiently rigorous dynamic theory of a focusing Cauchois diffraction spectrometer (Fig. 5) with an elastically bent crystal. The reflecting planes in this case can be either flat ($k = 0$) or bent on account of anisotropy. We obtain the shape of the line on the plane, perpendicular to CD, of the receiving slit, located on the focal circle of the instrument, of the detector D. Obviously, in this case $\eta = \rho\cos\vartheta$. Substituting this value in (5) and (8), we get

$$\xi(X) = \mp\frac{LX\tau}{Z\sigma}k\rho\cos\vartheta, \tag{9}$$

$$\frac{d\xi}{dX} = \mp\frac{L}{Z}\frac{\tau^2+X^2}{\sigma\tau}k\rho\cos\vartheta. \tag{10}$$

TABLE I. Comparison of the theoretical and experimental widths and intensities of the diffraction lines for variants 1–4 (Fig. 3).

	1		2		3		4	
	Theory	Experiment	Theory	Experiment	Theory	Experiment	Theory	Experiment
$\Delta\vartheta_\Sigma$, ang. sec.	37.6	37±1	23.4	24±1	23.4	23±1	43.5	40±1
$I_i(0)/I_1(0)$	1	1	0.31	0.37±0.04	1.54	1.4±0.1	0.21	0.25±0.02

Together with Eq. (6), these expressions provide the solution of our problem.

By way of a numerical example, Fig. 6 shows the line shape calculated for the right-hand (S_1D_1) and the left-hand (S_2D_2) "symmetrical" positions of the spectrometer with the crystal C_1 of the two-crystal variant described above (see Fig. 3): SiO_2, $01\bar{1}1$, $L = 0.16$ cm, $k = 0.88\cdot10^{-4}$ cm^{-1}, $\rho = 200$ cm, $P = 0.550$, $Z = 4.0$, $\mu = 9.82$ cm^{-1}, $E_x = 17.5$ keV. Just as above, only half of the profiles, which are symmetrical about the $\xi = 0$ axis, are drawn. The inessential α and β branches are shown magnified 100 and 1000 times are actually insignificant and at the given parameters. A strongly pronounced right–left asymmetry is observed and manifests itself not only in a difference between the areas under the lines (see Ref. 10, where the latter are considered, likewise within the framework of the Kato theory, theoretically and experimentally precisely for this instrument), but also in a difference between the widths as well as between the line shapes. We recall that we are considering a case with normal reflecting planes (prior to the bending of the crystal). We note also that the random-phase approximation which is frequently used presently in practical calculations of this type (the model of an ideal mosaic crystal) would yield right-hand and left-hand lines that are identical in intensity and in shape.

To the extent that the angles of the type OCD (Fig. 5)

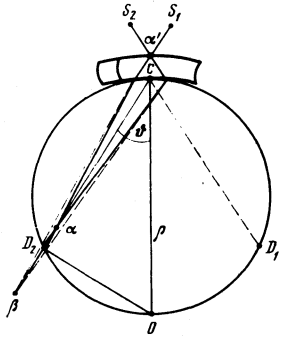

FIG. 5. Illustrating the analysis of the Cauchois focusing spectrometer and "point into point" focusing.

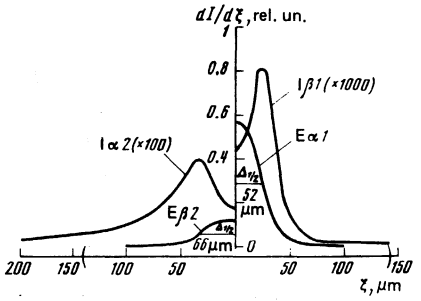

FIG. 6. Calculated line shapes for the Cauchois diffraction spectrometer (Fig. 5) in the right-hand (S_1D_1) and left-hand (S_2D_2) positions.

are equal, where C is an arbitrary point on the surface of the crystal, i.e., accurate to the so-called aperture aberration (see, e.g., Ref. 8), the result obtained above and in the present section is directly applicable also to the case of sources of finite size (up to several centimeters). Thus, the described calculation holds for a real focusing Cauchois spectrometer in the region of relatively soft radiation, where the dynamic theory of diffraction is valid.

B. "Point into point" focusing

An examination of Eq. (5) shows readily that at a definite value $\eta=\eta_f$ the value of ξ remains close to zero at values of X that are different from zero but satisfy the condition $X^2 \ll Z^2$. In other words, an almost pointlike image of the source S is produced at the focal distance η_f. For η_f we obviously obtain

$$\eta_f=\sin\vartheta \Big/ \left\{\frac{\operatorname{tg}\vartheta}{\rho}\pm k\left[\frac{Z^2+4}{Z^2}\right]^{1/2}\right\}, \tag{11}$$

where the plus and the minus signs pertain to the α and β branches, respectively. Only if we disregard the second term in the denominator do we get $\eta_f=\rho\cos\vartheta=\eta_K$ and the point focus is located on the focal circle of the Cauchois spectrometer. Actually, however, the second term is not negligibly small and its presence leads to focusing of the α branch somewhat closer to the crystal, and of the β branch somewhat farther (see points α and β in Fig. 5).

It is of interest to assess the limit to which η_f [relation (11)] tends as $\rho\to\infty$, i.e., when the crystal is straightened out. In this case $k\to 0, f\to 0, Z\to 0$ [see relations (1), (2), (3′)], and we get for η_f

$$\eta_f\to\pm\frac{Z}{2k}\sin\vartheta=\pm\frac{L\sin^2 2\vartheta}{2|\chi_g|\cos\vartheta\cos\pi^*}, \tag{11′}$$

where

$$\chi_g=r_e\lambda^2F_g/\pi V,$$

which is identical to the expression for the focal distance in diffraction focusing by an ideal crystal after Afanas'ev and Kon (see Refs. 4 and 5). The minus sign denotes in this case the onset of an imaginary focus for the β branch on the other side of the crystal, but at the same distance as for the real focus for the α branch.

We note in conclusion of this subsection that a situation that differs from the considered one only in the direction of propagation of the rays was already investigated by Petrashen' and Chukhovskii.[3] This comparison makes particularly obvious the close relation between the types of focusing considered in Refs. 1–3 and in Refs. 4–6 (see the Introduction).

C. "Point into parallel beam" focusing

It follows from (11) that if the condition

$$\operatorname{tg}\vartheta/\rho=\mp k[(Z^2+4)/Z^2]^{1/2} \tag{12}$$

is satisfied the focal distance becomes infinite, and the radiation from a point source diffracted by the bent crystal forms an almost parallel beam. In the geometry of Fig. 5 such a beam is produced by the β branch, but a similar effect is obviously attainable also for the α branch if the direction of the bending of the crystal is reversed. At $k=0$ we have $Z=0$ and the condition (12) can be reduced to the form

$$\frac{1}{\rho}=\frac{2r_ed^2F_g}{\pi VL}\cos\pi^*. \tag{12′}$$

Thus, the condition for the focusing in question is satisfied in this case regardless of the wavelength of the diffracted radiation (for the polarization $\cos\pi^*=1$); a point source emitting several monochromatic lines produces a corresponding number of rather weakly diverging monochromatic beams, each at its own Bragg angle. Typical bending radii ρ of millimeter-thickness ($L=0.1$ –0.2 cm) used for x rays amount to tens and hundreds of meters. If the ray propagation direction is reversed, then the situation is reminiscent of the Indenbom focusing.[2]

In the general case, i.e., at nonzero values of k and Z, the condition (12) turns out to depend on the wavelength of the diffracted radiation, i.e., for each crystal there is some "resonant" wavelength (radiation energy) for which focusing into a parallel beam is realized.

Substituting (12) in (5) and (8) and then using (6), i.e., proceeding in exactly the same manner as in the example of Sec. 3A, we easily calculate $\xi(X,\eta), d\xi/dX$ and $dI/d\xi=f(\xi)$. The result of such a calculation of the shape of a spot due to a point source of Fe^{57} ($E_\gamma=14.4$ keV) on a screen placed 1 m and 1 km away from the crystal (11$\bar{2}$2, $L=0.16$ cm, $\rho=200$ cm, $k=12.2\cdot10^{-4}$ cm^{-1}) is shown in Fig. 7. It is seen that the parallelism of the beam can actually be quite high.

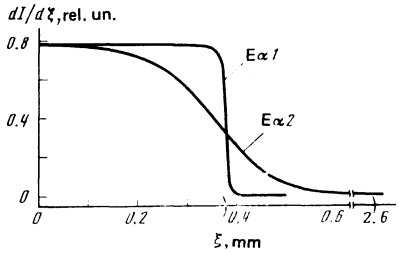

FIG. 7. Calculated shapes of the spots on the screens located at a distance 1 m (Eα1) and 1 km (Eα2) from the crystal. The brackets indicate the values $\xi_m=0.379$ mm for $\eta=1$ and $\xi_m=2.6$ mm for $\eta=1$ km [relation (15) at $\varepsilon=0.1$].

CONCLUSION

In conclusion we examine the factors that limit the applicability of the foregoing description.

1. The Kato eikonal theory used by us is known to be only an approximation of the rigorous theory. The conditions under which the correction terms are small, i.e., the eikonal approximation is accurate enough, were obtained, for example, in Ref. 11. They can be easily reduced to the form

$$t_e/[1-(X/Z)^2]^{1/2} \leqslant \varepsilon L, \quad 2t_e k \leqslant \varepsilon \Delta\vartheta_B, \tag{13}$$

where

$$t_e = \frac{\cos\vartheta}{\cos\pi^*} \frac{V}{r_e (F_g F_{\bar{g}})^{1/2} \lambda}$$

is the primary damping distance, and $\varepsilon < 1$ (at $\varepsilon \leqslant 0.1$ the correction terms do not exceed 3%).

The physical meaning of conditions (13) in this form is clear. The first is obviously simply the thick-crystal condition: the effective length of the primary damping (with allowance for the distance between the point of emergence of the ray and the edge of the Bormann delta) should be less than the thickness of the crystal. The second is a peculiar adiabaticity condition and reduces to the requirement that the angle of rotation of the tangent to the bent reflecting planes, over the primary damping thickness, be small compared with the Bragg diffraction width $\Delta\vartheta_B$. For sufficiently soft radiation, for example for x rays with energy 10–20 keV, both conditions are easy to satisfy. The brackets on Figs. 4, 6, and 7 indicate the limiting values of the abscissas ($\Delta\vartheta_D$ or ξ) corresponding to the first condition of (13) at $\varepsilon = 0.1$.

2. More significant limitations are imposed by the mosaic character of the real single crystals, which apparently introduces a scatter in the angular distributions of the rays, on the order of the width of the distribution over the angles ω_g of the mosaic blocks of the crystal. For the better natural crystals the latter, to our knowledge, is not less than 0.3–0.5″. For synthetic single crystals of silicon (or germanium) with an extremely small amount of impurities and dislocation densities one can probably attain presently mosiac angles of the order of $\omega_g \approx 0.1''$.

Allowance for mosaic angles $\omega_g \leqslant 0.5''$ has practically no effect on the results of the type shown in Figs. 4 and 6. In the case of "point into point" focusing the mosaic structure makes it obviously impossible to obtain images with dimensions smaller than $\omega_g \eta_f$, i.e., of the order of $0.1 \cdot 5 \cdot 10^{-6} \cdot 200 \approx 1$ μm, thereby limiting reasonable dimensions of the detector slit ($\Delta D \geq 1$ μm) and the resolving powers of spectrometers based on this principle. In the case of "point into a parallel beam" focusing, allowance for the mosaic structure leads to a broadening of the "spot" at a distance of a kilometer by $\Delta\xi \approx 0.1 \cdot 5 \cdot 10^{-6} \cdot 10^5 = 0.5$ mm, i.e., to approximate doubling of its width (see Fig. 7).

Thus, the different versions of diffraction focusing makes it possible to get around the diffraction Bragg width, which is frequently considered to be the limit of the angular resolution of diffraction instruments, and is limited apparently only by the mosaic structure of the single crystals; a study of the latter is a complicated matter, but as can be seen, a worthwhile technological task.

[1)] Starting from Fig. 1, it is easy to estimate the maximum phase differences of the interfering beams at $\Delta\Phi_m \approx 2\pi L d^{-1} \operatorname{tg}\vartheta$, and at typical (see below) crystal thicknesses $L \approx 0.1$–0.2 cm and interplanar distances $d \approx (1/2) \cdot 10^{-8}$ cm and at $\operatorname{tg}\vartheta \approx 0.1/0.5$ this yields $\Delta\Phi_m \approx 10^6 \cdot 2\pi$. Thus, one can expect $\approx 10^6$ fringes within the limits of the widths of the diffraction maxima.

[2)] The quantity $\Delta\vartheta_a$ in (3) is the angle of deviation from the exact Bragg direction on the exit face of the crystal. It is more convenient to choose as a reference (see the η axis in Fig. 1) the exact Bragg direction on a neutral plane, i.e., at the midsection of the plate. This was in fact done for Eq. (3′). The values $\Delta\vartheta_0$ and $\Delta\vartheta_a$ are connected by the obvious equation $\Delta\vartheta_0 = \Delta\vartheta_a - kL$.

[3)] In the geometry of Fig. 1, when the K_0 radiation is incident on a concave surface of a bent reflecting plane, the important role is played by the α branch.

[4)] In the comparison with experiment one must take into account the finite angular resolution of the analyzing flat crystal C_2 (Fig. 3), which is determined by its Bragg width $\Delta\vartheta_B = 2''$. Strictly speaking, what should be compared with experiment are the convolutions of the theoretical curves with the reflection curve of the analyzing crystal. This, however, has no practical effect on the parameters that are quantitatively compared in the table, and is significant only in the region of the singularities, the weaker of which "vanish," making the theoretical picture less significant.

[1] A. Authier, A. D. Milne, and M. Sauvage, Phys. Status Solidi **26**, 469 (1968).

[2] V. L. Indenbom, I. Sh. Slobodetskiĭ, and K. G. Truni, Zh. Eksp. Teor. Fiz. **66**, 1110 (1974) [Sov. Phys. JETP **39**, 542 (1974)].

[3] P. V. Petrashen' and F. N. Chukhovskiĭ, Quasiclassical x-ray scattering by an elastically bent crystal, Preprint, Crystallography Inst. USSR Acad. Sciences. Pis'ma Zh. Eksp. Teor. Fiz. **23**, 385 (1976) [JETP Lett. **23**, 347 (1976)].

[4] A. M. Afanas'ev and V. G. Kon, Fiz. Tverd. Tela (Leningrad) **19**, 1775 (1977) [Sov. Phys. Solid State **19**, 1035 (1977)].

[5] V. V. Aristov, V. I. Polovinkina, I. M. Shmyt'ko, and E. V. Shulakov, Pis'ma Zh. Eksp. Teor. Fiz. **28**, 6 (1978) [JETP Lett. **28**, 4 (1978)].

[6] V. D. Koz'mik and I. P. Mikhaĭlyuk, Pis'ma Zh. Eksp. Teor. Fiz. **28**, 673 (1978) [JETP Lett. **28**, 637 (1978)].

[7] N. Kato, J. Phys. Soc. Jpn. **19**, 971 (1964).

[8] O. I. Sumbaev, Kristall-difraktsionnye gamma-spektrometry (Crystal-Diffraction Gamma Spectrometers), Atomizdat, 1963.

[9] O. I. Sumbaev, Zh. Eksp. Teor. Fiz. **54**, 1352 (1968) [Sov. Phys. JETP **27**, 724 (1968)].

[10] Yu. S. Grushko, E. G. Lapin, O. I. Sumbaev, and A. V. Tyunis, Zh. Eksp. Teor. Fiz. **74**, 2280 (1978) [Sov. Phys. JETP **47**, 1185 (1978)].

[11] T. Katagawa and N. Kato, Acta Crystallogr. A **30**, 830 (1974).

Translated by J. G. Adashko